LANGMUIR

Article

pubs.acs.org/Langmuir

Mechanistic Studies on the Self-Assembly of PLGA Patchy Particles and Their Potential Applications in Biomedical Imaging

C. Salvador-Morales,[*,†,‡] Binal Brahmbhatt,[†,‡] V. Márquez-Miranda,[§] I. Araya-Duran,[§] J. Canan,[∥] F. Gonzalez-Nilo,[§] C. Vilos,[§,⊥] J. Cebral,[†,‡] F. Mut,[†,‡] R. Lohner,[#] B. Leong,[▽] G. Sundaresan,[▽] and J. Zweit[▽]

[†]Bioengineering Department, George Mason University, 4400 University Drive, MS 1G5, Fairfax, Virginia 22030, United States

[‡]Krasnow Institute for Advanced Study, George Mason University, 4400 University Drive, MS 2A1, Fairfax, Virginia 22030, United States

[§]Center for Bioinformatics and Integrative Biology, Facultad de Ciencias Biologicas, Universidad Andres Bello, Santiago, Chile 8370146

[∥]Fundación Fraunhofer Chile Research, M. Sanchez Fontecilla 310, Las Condes, Chile 7550296

[⊥]Center for Integrative Medicine and Innovative Science, Faculty of Medicine, Universidad Andres Bello, Santiago, Chile 8370146

[#]Center for Computational Fluid Dynamics, College of Sciences, George Mason University, Fairfax, Virginia 22030, United States

[▽]Center for Molecular Imaging, Department of Radiology, Virginia Commonwealth University, Richmond, Virginia 23298, United States

Supporting Information

ABSTRACT: Currently, several challenges prevent poly(lactic-*co*-glycolic acid) (PLGA) particles from reaching clinical settings. Among these is a lack of understanding of the molecular mechanisms involved in the formation of these particles. We have been studying in depth the formation of patchy polymeric particles. These particles are made of PLGA and lipid−polymer functional groups. They have unique patch−core−shell structural features: hollow or solid hydrophobic cores and a patchy surface. Previously, we identified the shear stress as the most important parameter in a patchy particle's formation. Here, we investigated in detail the role of shear stress in the patchy particle's internal and external structure using an integrative experimental and computational approach. By cross-sectioning the multi-patch particles, we found lipid-based structures embedded in the entire PLGA matrix, which represents a unique finding in the PLGA field. By developing novel computational fluid dynamics and molecular dynamics simulations, we found that the shear stress determines the internal structure of the patchy particles. Equally important, we discovered that these particles emit a photoacoustic (PA) signal in the optical clinical imaging window. Our results show that particles with multiple patches emit a higher PA signal than single-patch particles. This phenomenon most likely is due to the fact that multipatchy particles absorb more heat than single-patchy particles as shown by differential scanning calorimetry analysis. Furthermore, we demonstrated the use of patchy polymeric particles as photoacoustic molecular probes both *in vitro* and *in vivo* studies. The fundamental studies described here will help us to design more effective PLGA carriers for a number of medical applications as well as to accelerate their medical translation.

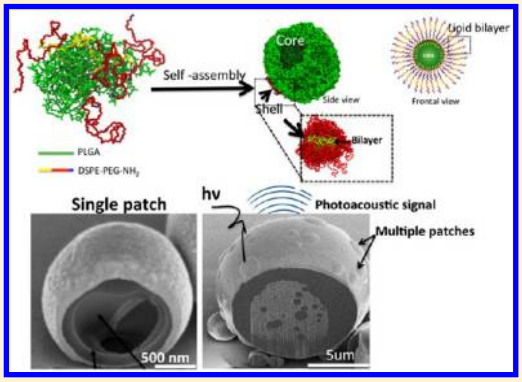

INTRODUCTION

Patchy particles are a class of anisotropic particles that have one or more surface-exposed domains with different surface chemistry relative to the rest of the particle.[1] Such particles can be advantageous for a number of applications such as imaging, drug delivery, theranostics, vaccines, and tissue engineering.[2] For example, as a theranostic, patchy particles allow the combination of fully decoupled modalities for imaging and therapy. In tissue engineering, a patchy surface can uniquely advance medicine as it allows functionalizing the patches with multiple ligands to target different types of cells. In biomedical imaging, the patch cluster effect can significantly enhance the imaging signal due to the high density of imaging molecules in a well-defined area of the carrier.

The anisotropic feature of nano- and micrometer-size patchy particles has been formulated using several techniques including the template-assisted fabrication,[3−5] electrified jetting,[6,7] glancing angle deposition,[8,9] lithography,[10,11] and phase segregation[12,13]. In our patchy particles, the anisotropic

Received: June 10, 2016
Published: July 29, 2016

DOI: 10.1021/acs.langmuir.6b02177
Langmuir 2016, 32, 7929−7942

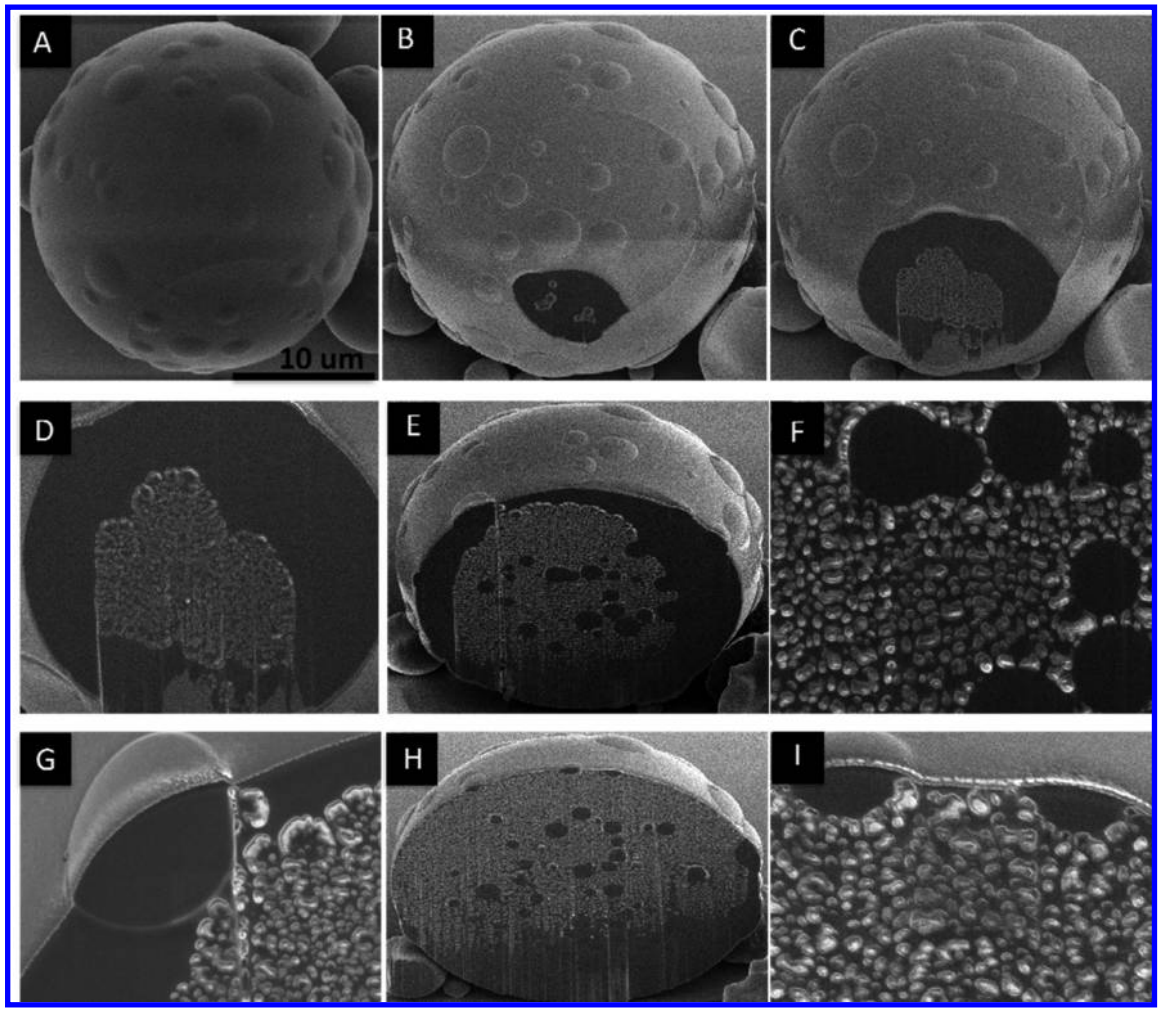

Figure 1. Cross-sections of particles with multiple patches. (A–I) Cross-sections revealing the presence of lipid-based structures embedded in the entire particle's core. The step size between the cross-sections was 500 nm. (F) Close-up of the lipid-based structures embedded in the particle core. (G) Arrangement of the lipid-based structures close to the patch. (H) Half of the particle's core completely covered by lipid-based structures. (I) Close-up of the lipid-based structures near the patch. It is clear that the lipid-based structures found in the particle's core have a different arrangement from that of LPFGs in the patch or patches.

attribute arises from the spontaneous and unexpected unique arrangement of lipid-PEGylated functional groups (LPFGs) on the particle's surface.[14] LPFGs such as 1,2-distearoyl-*sn*-glycero-3-phosphoethanolamine-*N*-[R (poly(ethylene glycol))-2000] (DSPE-PEG-R; R = NH_2, maleimide, and so on) have been extensively used as building blocks for the synthesis of nanotherapeutics because their end-terminal functional groups can be functionalized with a variety of organic and/or inorganic molecules.[15−23] Furthermore, LPFGs offer the advantage of synthesizing multifunctional nanoparticles, in which control over the number and ratio of functionalities on the particles' surface, can be achieved without the need of orthogonal chemical reactions.[24]

To accelerate clinical trials of polymeric particles, such as those made of poly(lactic-*co*-glycolic acid) (PLGA) polymer, a number of challenges need to be overcome. Among these, is a lack of understanding of the mechanisms involved in the formation of these particles at the molecular level. Moreover, the driving force of the self-assembly process, which is commonly implicated in the formation of particles synthesized using nanoprecipitation or double emulsion methods, is different at the nano- and micrometer-size scales. The self-assembly process depends on several factors, including mechanical and chemical parameters such as shear stress and solvent composition among others, which very often are not fully studied in detail during the particles'synthesis. The purpose of this work is to synthesize patchy polymeric particles by addressing, in depth, these fundamental issues. Thus, in this work, we provide a mechanistic study of the self-assembly process of PLGA and LPFGs that renders particles with a patchy surface and hollow or solid core. Equally important, we report the *in vitro* and *in vivo* biomedical imaging application of patchy polymeric particles.

Previously, we reported the spontaneous formation of heterogeneous patches on polymeric particle's surface,[14] as well as the mechanism behind the formation of these new anisotropic particles.[25] We found that the shear stress the polymer blend undergoes, during the emulsification step in the particle's synthesis, is the most important parameter for the formation of particles with single patches. Here, we further investigated the role of the shear stress in the formation of the internal and external morphology of lipid−polymeric patchy particles with single and multiple patches, using an integrative experimental and computational approach. The ability to detect and control the parameters that play a key role in the formation of patchy particles will enable better control of their

DOI: 10.1021/acs.langmuir.6b02177
Langmuir 2016, 32, 7929−7942

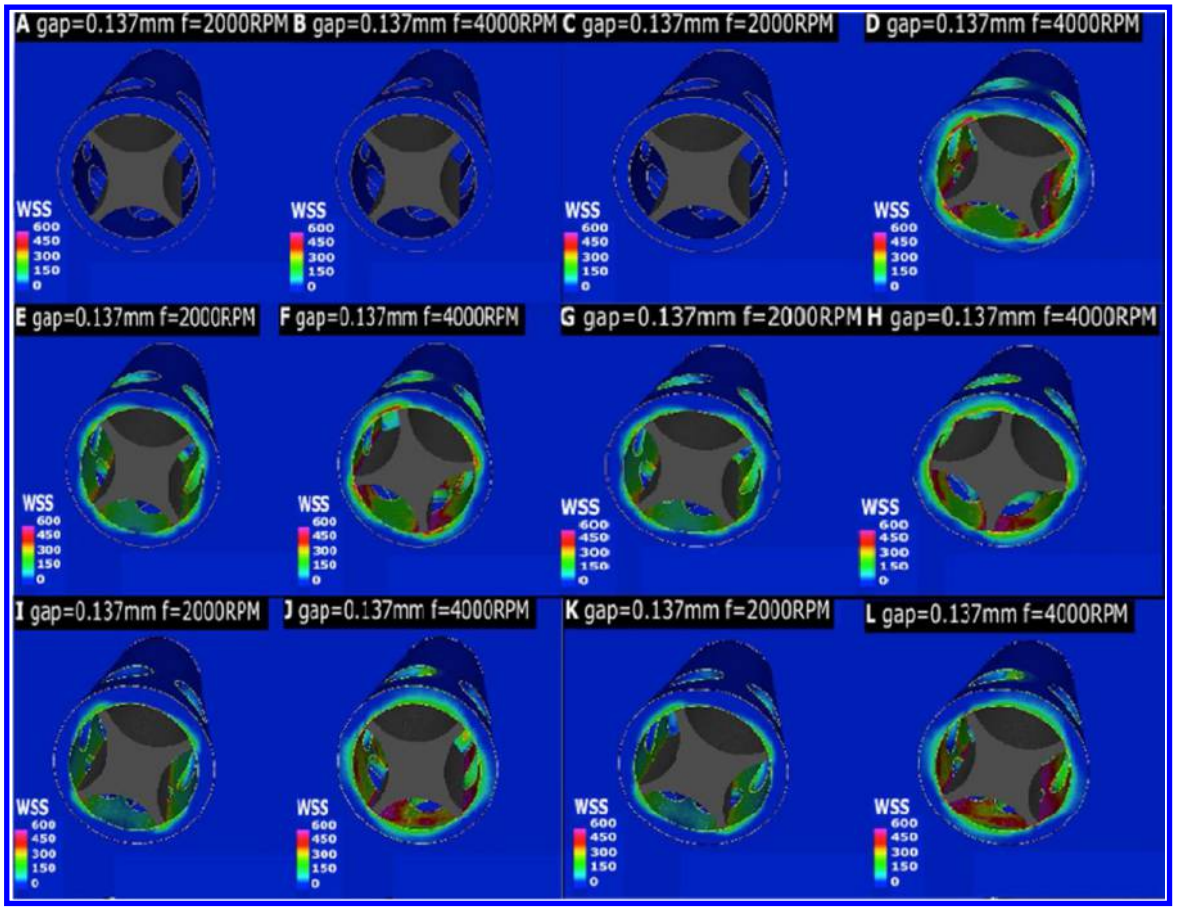

Figure 2. Computational fluid dynamics (CFD) simulations. CFD simulations were developed to determine the wall shear stress between the homogenizer's workhead and rotor shaft. Comparison of the wall shear stress at 2000 rpm (left side) and 4000 rpm shear rate (right side). The wall shear stress at 2000 rpm is very low compared with that at 4000 rpm as its value is 150 dyn/cm^2 and between 450 and 600 dyn/cm^2, respectively. The CFD simulations were developed using a gap size of 0.137 mm.

physicochemical properties. Thus, these fundamental studies will also enable us to improve the loading efficiency, release kinetics, batch control, scalability, and customization of the carrier according to the intended application, as well as, tuning the recently revealed photoacoustic properties of these particles.

RESULTS AND DISCUSSION

Patchy Particle's Internal Structure. To further understand the role of the shear stress in patchy particle formation, we synthesized particles at different shear stress rates: 2000 and 4000 rpm. We found that multiple and single patches were formed using high shear mixer sets at 2000 or 4000 rpm, respectively. Previously, by cross-sectioning single-patch particles, we discovered and reported that these particles have a hollow core.[25] Using the same rationale, we cross-sectioned the particles with multiple patches. The cross-sections revealed that these particles have a solid core with entrapped lipid-based structures (Figure 1). As we gradually cross-sectioned the particle's core, we observed that the lipid-based structures are embedded in the entire polymer matrix, and their presence is even more prominent in the middle of the particle's core as shown in Figure 1H. Moreover, it is worth noting that the lipid-based structures are only observed in the particle's core and not in the patch or patches. This finding suggests that although the lipid-based structures in the particles' core are made of LPFG, their arrangement is different from that in patch or patches. In fact, the lipid-based structures in the particle's core tend to separate from the patch or patches.

Computational fluid dynamics (CFD) simulations developed to determine the wall shear stress between the homogenizer's workhead and rotor shaft showed that the wall shear stress at 2000 rpm is low (i.e., 450 dyn/cm^2) compared with that at 4000 rpm (i.e., between 450 and 600 dyn/cm^2) (Figure 2). Based on these results, it is clear that the shear stress rate determines whether the particle's internal structure is solid or hollow. Nevertheless, CFD is not enough to fully understand the formation of the particles' internal morphology. Therefore, we performed molecular dynamics (MD) simulations to gain insights about the self-assembly process of PLGA and LPFG. Due to the high number of atoms needed to develop MD of a microparticle of an average size of 2 μm in diameter, we had to perform MD of a nanoparticle of 18 nm in diameter. This nanoparticle was made of PLGA. The two monomers of PLGA, lactic acid and glycolic acid, were built and later replicated at random, making a total of 419 lactic acids (76%) and 131 glycolic acids (24%) monomers for a single chain of PLGA (see Full-Atomistic Molecular Dynamics Simulation and Supporting Information).

In the first place, full-atomistic MD simulation was carried out to elucidate the nature of the interactions that drive the formation of DSPE-PEG-NH$_2$/PLGA complex. To achieve this goal, pair interaction energy values were obtained from DSPE (tails)-PLGA, PEG-PLGA, and PEG-DSPE (tails) fragments, of

DOI: 10.1021/acs.langmuir.6b02177
Langmuir 2016, 32, 7929−7942

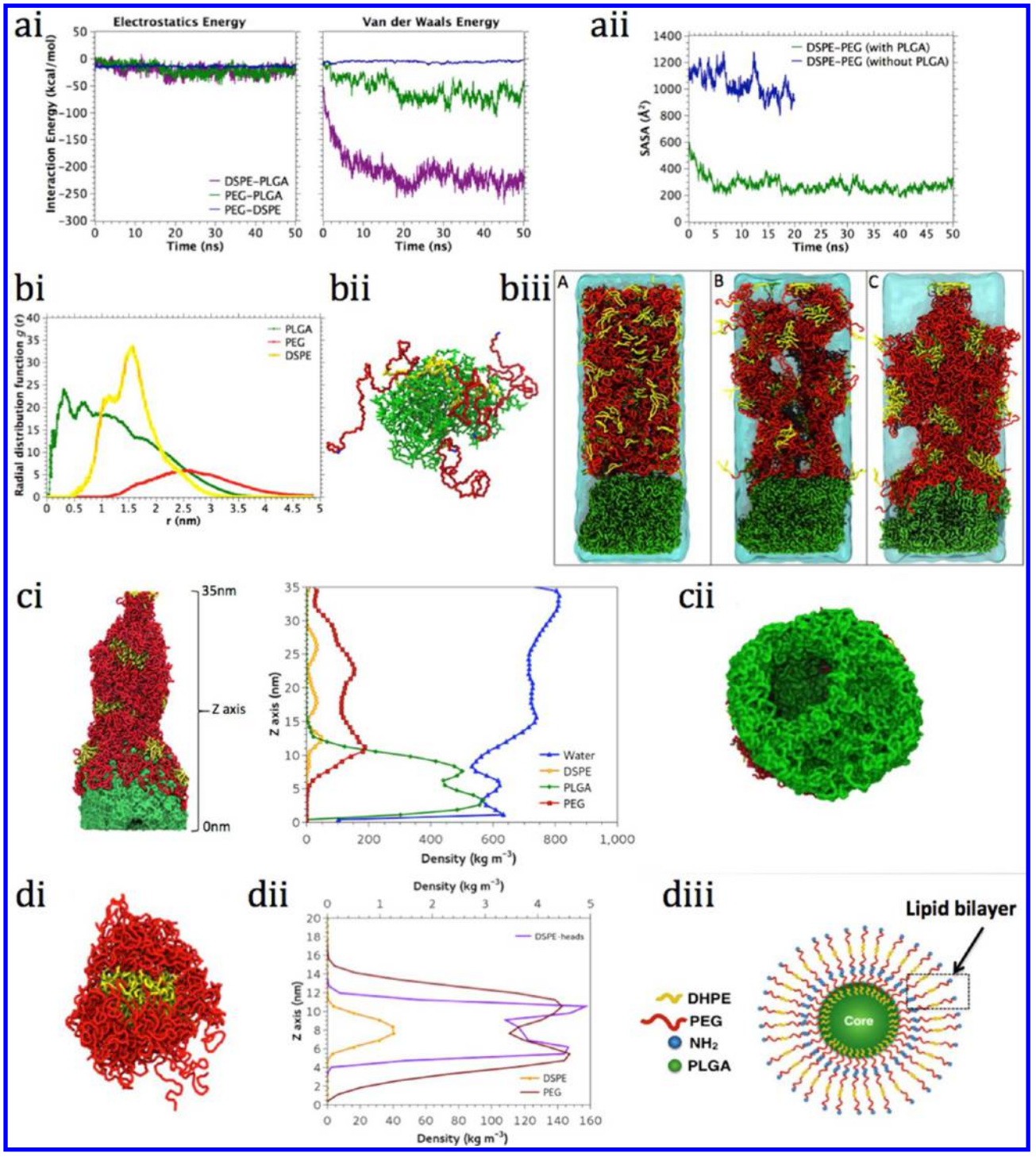

Figure 3. Molecular dynamics simulations. (a(i)) van der Waals and electrostatics interaction energy of PEG-DSPE, PEG-PLGA, and DSPE-PLGA polymers. (a(ii)) Solvent accessible surface area (SASA) of DSPE-PEG in the presence and absence of PLGA. (b(i)) Radial distribution of DSPE (tail), PEG, and PLGA with respect to the center of mass of the nanoparticle composed of these polymers, taken from a full-atom molecular dynamics simulation. (b(ii)) Snapshot of the last frame of MD full-atom trajectory, showing DSPE-PEG and PLGA components of the nanoparticle. (b(iii)) Self-assembly process of DSPE-PEG polymers (top) into the surface of the PLGA nanoparticle (bottom): (A) Initial step of the simulation, where the DSPE-PEG polymers were placed at random into a water box; (B) at 250 ns of coarse-grained molecular simulation, monomers starting to agglomerate; (C) toward the end, DSPE hydrophobic sections that form bilayers. (c(i)) Snapshot of the last frame of the coarse-grained simulation of the self-assembly of DSPE-PEG-polymer into the surface of PLGA block (left). Density (kg m^{-3}) of chemical groups in the coarse-grained system, containing water, DSPE, and PEG (separately) and PLGA (right graph). (c(ii)) Cartoon of a single-patch particle with a hollow core. (d(i)) Cartoon of the formation of the particle's patch showing the formation of the lipid bilayer. (d(ii)) Density (kg m^{-3}) of chemical groups of a DSPE-PEG block, considering DSPE tails, PEG, and DSPE head groups. (d(iii)) Schematic drawing of patchy particles showing the formation of a lipid bilayer in the particle's surface.

DOI: 10.1021/acs.langmuir.6b02177
Langmuir 2016, 32, 7929−7942

the same number of atoms, taking into account the last part of the simulation. This calculation was performed using NAMD Energy plugin included in VMD software. As hypothesized, the van der Waals energy between the polymers is significantly higher than the electrostatic energy (Figure 3a(i)). MD revealed that the most favorable van der Waals interaction occurred between DSPE and PLGA as the interaction between the DSPE, and PEG sections are displaced as shown in Figure 3a(i). The DSPE-PEG interaction was more relevant at the beginning of MD, but that interaction changed over time as the molecules were arranged. Similarly, PEG and PLGA also showed a favorable van der Waals interaction but not as strong as DSPE-PEG. At the same time, the calculation of solvent accessible surface area (SASA) ratifies that DSPE-PEG remains more protected from the environment (lower values of SASA) being in contact with PLGA polymers (Figure 3a(ii)). Furthermore, as it can be observed from a radial distribution function (RDF), DSPE tails are partially embedded into PLGA nanoparticle, while some sections are interacting with PEG polymers (Figure 3b(i)). The PEG section is also in part buried into PLGA. Interestingly, DSPE appears as an interface between PEG and PLGA, while PEG tends to displace more toward the surface. Figure 3b(ii) illustrates a snapshot of the last frame of the MD trajectory. In this picture, it is clear how PLGA and DSPE-PEG-NH_2 interact with each other between the hydrophobic regions. Knowing the interaction between PLGA and DSPE-PEG-R will enable more control on the particle's surface chemistry and, therefore, will potentially help improve their *in vivo* performance, as the particle's surface chemistry plays a significant role in the protein−corona effect. Moreover, using the MD simulations, we can vary the PEG's molecular weight and molar ratio with respect to the PLGA to predict the particle's surface chemistry. Since little information is available today about PLGA and DSPE-PEG-R interaction, these simulations substantially contribute to the field of PLGA nanoparticle's synthesis.

By developing coarse-grained MD, we aimed to understand the formation of the hollow aspect of the particle's core. In this type of simulation, we incorporated a variable pressure to emulate the shear stress that the polymer blend undergoes during the emulsification step of the particle's synthesis. To start the simulation, DSPE-PEG polymers were placed at random, in a water box, on the top of the PLGA nanoparticle (Figure 3b(iii)). As the simulation was carried out, hydrophobic DSPE tails started to agglomerate (Figure 3b(iiiA)), while water penetrated both PEG sections and PLGA block. Toward the end of the simulation, we observed the formation of bilayers, which are composed of DSPE molecules, while DSPE-PEG polymers collapsed into the surface of the PLGA nanoparticle due to the effects of the high pressure applied to the system (Figure 3b(iiiC)). Analysis of the system density over the last frame of the simulation (Figure 3c(i) image and graph) shows that PLGA density encompasses the area 0 nm < z < 15 nm. Interestingly, the density of the nanoparticle does not constitute a rigid core. Specifically, the area where the density decays (3 and 8 nm in the z-axis) coincides with an increase in the density of water in that zone, in agreement with our observation of the penetration of water into the nanoparticle. Moreover the fact that the density of water is >0 along the block demonstrate that water can penetrate PLGA and PEG sections. As a result of this phenomenon, the nanoparticle formed by the PLGA polymer shows some cavities inside, denoting the entry of water. Experimentally, we found that particles with single patches have a hollow core. Initially, we hypothesized that the particle's hollow core was formed because the shear stress force that the polymer blend undergoes during the emulsification step in the particles synthesis, overcomes the van der Waals interaction that exists between DSPE and PLGA. Although the cavity of the particles was observed in MD when the nanoparticle's core is already formed, it is clear that the pressure parameter incorporated into the MD or the shear stress force applied during the emulsion of the polymers causes the particle's hollowness.

Patchy Particle's External Structure. MD also rendered information about the arrangement of the LPFGs in the particle's surface. These MD show that the hydrophobic tails (DSPE) distribution display regular peaks, indicating the formation of bilayers along the block (Figure 3ci graph). A single peak of DSPE is near the surface of PLGA nanoparticle (z = 12), showing tails that collapse into its surface (Figure 3c(i), graph). Meanwhile, PEG sections are distributed in the same area as DSPE, 5 nm < z < 35 nm. Noticeably, where the density of PEG decays, the density of water increases, showing that this polymer is acting as a sponge. In fact, the ground section of the block, encompassing the area 0 < z < 13, is similar compared with the nanoparticle formed along the full-atom molecular dynamics simulation. In this area, PEG and PLGA compete in the interaction with DSPE tails.

To facilitate the analysis of the bilayers formed during the coarse-grained simulation, we selected a small block of DSPE-PEG polymers from the final aggregate (Figure 3d(i)). As can be deduced from the density profile (Figure 3d(ii)), DSPE tails occupy the area 5 nm < z < 11 nm. DSPE head groups (defined by -NH_3^+ groups) represented by two peaks (purple line), in the regions of 4−6 and 10−12 nm, denote the interfacial area of the lipids, showing the typical profile of a bilayer. PEG polymers are distributed in the upper and lower parts of the bilayer, which decreased their density in the DSPE bilayer area. A schematic representation of the arrangement of DSPE-PEG-NH_2 on the particle's surface can be observed in Figure 3d(iii). MD simulations confirm that DSPE fragments of the LPFGs form not only the interface between PLGA and DSPE-PEG-NH_2 but also inform about the formation of a bilayer on the particle's surface. Moreover, MD shows that part of DSPE and PEG are buried in PLGA. The structural information about the arrangement of the LPFG in the particle's surface is extremely necessary to achieve high control on patchy particles' surface chemistry. Also, this information can be relevant for the selection of payloads for a particular application.

Furthermore, the MD simulations show that some molecules of H_2O are also entrapped in the particle's core whether the core is solid or hollow. Moreover, because of the effect of the pressure, and due to the fact that the water is incompressible, several holes are formed in the PLGA nanoparticle. At the same time, the lipid and polymer molecules offer more interstice that can suffer more compression than bulk water. When the shear stress force is low, the van der Waals interaction between PLGA and DSPE-PEG-NH_2 is strong, leading to the formation of a solid particle's core with entrapped lipid-based structures. The lipid-based structures formed in the particle's core are presumably of a particular arrangement of lipid−polymer-based functional group. MD showed how the DSPE fragment of the DSPE-PEG-NH_2 interacts closely and preferentially with the lactic monomer, which is not surprising because the DSPE fragment and lactic acid are hydrophobic (see Supporting Information). Moreover, in the presence of low shear stress,

DOI: 10.1021/acs.langmuir.6b02177
Langmuir 2016, 32, 7929−7942

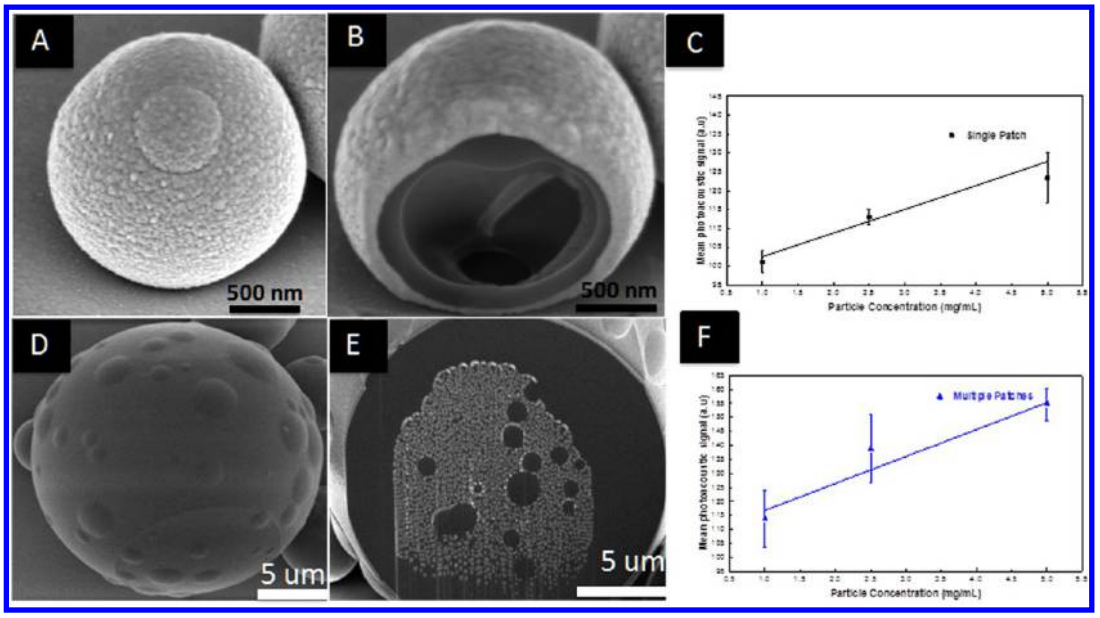

Figure 4. Intrinsic photoacoustic properties of patchy polymeric particles. Particles with different external and internal structures. (A, B) Particles with a single patch, thin shell, and hollow core. (D, E) Particles with multiple patches with a solid core and lipid−polymer-based functional groups entrapped in the core. (C−F) Direct relationship between PA signal and particle's concentration. As the particle's concentration increases, the patchy particle's PA signal increases.

many DSPE-PEG-NH_2 get entrapped in the particle's core because of the high diffusion coefficient of the DSPE fragment that enhances and facilitates its interaction and penetration into the PLGA copolymer. Interestingly, polymeric particles with multiple patches are very unique materials because their external surface is very different from their internal morphology, which provides several advantages. For example, the outer surface has multiple domains that can be further functionalized with organic or inorganic molecules, while the internal morphology can be exploited for imaging purposes because these particles emit a photoacoustic (PA) signal. The natural PA signal of these particles is discussed in detail in the following section of this work. Furthermore, it is important to mention that the particles with multiple patches are quite rare in the colloidal chemistry field because until today literature does not report particles with multiple patches formed by both PLGA and LPFGs. As of now, most of the papers published on PLGA particles report particles with a hollow and solid core.[26,27] Few publications report polymeric particles with multiple patches.[28−30] Among these works, some of them report patches that are formed by the partial or complete segregation of two different polymers such as poly(lactic acid) and polystyrene.[28] Other papers report PLGA particles with a solid core but without lipid-based structures.[31] Recently, another research group has reported a strategy to synthesize PLGA particles with water molecules inside the core.[32] This scientific evidence suggests that particles with single and multiple patches are unique in the field of nanoparticles and microparticles. Thus, the next question was to investigate whether these particles with singular internal morphology have attractive optical properties.

Biomedical Applications of Patchy Polymeric Particles. We discovered that these patchy polymeric particles possess unique optical properties. Specifically, they produce a PA signal in a dose-dependent fashion in the near-infrared (near-IR) region (i.e., 600−950 nm) as shown in Figure 4. *In vivo*, it is known that the near-IR (700−1100 nm) is where the influence of the main tissue absorbing components, oxy- and deoxyhemoglobin (maximum < 600 nm) as well as water (maximum > 1150 nm) is minimal. Therefore, this region of the spectrum is considered as the ideal optimal imaging window.[33] The fact that these particles can emit a PA signal in a relevant imaging window is a very exciting discovery because, to the best of our knowledge, there are no other polymeric particles that can emit a natural PA signal. Particles with multiple patches induce a higher PA signal than patchy particles with single patches at lower concentrations as shown in Figure 4. This phenomenon must be likely due to the ability of particles with multiple patches to absorb more light than single-patch particles. In the case of particles with single patches, the hollow core that is full of water will likely dissipate energy from the PA signal at the moment in which the PA measurement is taken in the phantom. From the molecular level perspective, we believe that particles with multiple patches might be better natural photoacoustic contrast agents than particles with single patches because the multipatch particles can offer a larger surface area to the solvent in the self-assembly process that generate the multiple patches.

By conducting differential scanning calorimetry studies, we investigated the thermal properties of these particles (Figure 5). Both particles exhibit a relatively similar melting point temperature. The melting temperature of patchy particles with multiple patches is 59 °C whereas the melting point temperature of particles with single patches is 57 °C. There are only two degrees of difference between them. Furthermore, single-patch particles have a crystallization temperature (T_c) of approximately 2.2 °C while the multiple domain patchy particles have a T_c of approximately −5 °C. The one sharp peak for each sample indicates that these samples are pure. Since the peaks are not broad, both samples are not partially crystalline polymers but are amorphous. Since both samples contain no α-nuclei, they have no crystallization peak and no α-melting peak. The baseline shifts lower toward the endothermic direction after the peak for both samples due to the increased

DOI: 10.1021/acs.langmuir.6b02177
Langmuir 2016, 32, 7929−7942

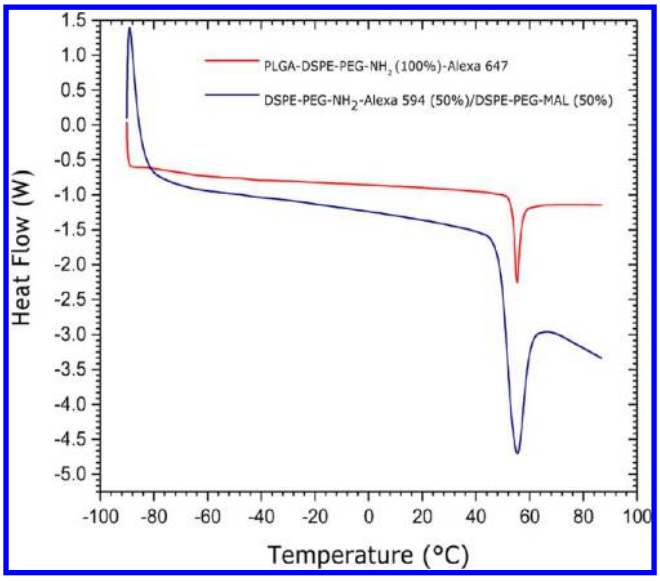

Figure 5. DSC thermogram of particles with single and multiple patches. Both particles exhibit a relatively similar melting point temperature. Multipatch particles have higher enthalpy than single-patch particles with means that the former absorbs more heat than particles with individual patches.

heat capacity of the sample. The biggest difference between particles with single and multiple patches is the enthalpy, the area under their peaks. Particles with multiple patches exhibit higher enthalpy than those with single patches, which means that the former absorb more heat than particles with individual patches. This thermal profile correlates well with the intrinsic photoacoustic properties of patchy particles. High enthalpy seems to render higher photoacoustic signal. We aim to enhance or modulate the patchy polymeric particles' PA signal by functionalizing their patch or patches with gold nanorods (GNRs) or by tuning their internal properties. For example, the multiple-patch particles can display an unparalleled PA imaging performance because of the functionalization of their patch and particles' surface with GNRs as shown in Figure 6A,B. Figure 6C shows a very strong PA signal from multipatch particles even at deep regions in the phantom.

To investigate the differential internalization of patchy polymeric particles (PPPs) in KB3-1 ovarian cancer cells, we synthesized single-patch particles with folic acid (FA) as the targeting moiety and labeled with NBD-cholesterol. It is known than the folate receptor α is overexpressed in a number of cancer cells including breast and ovarian cancer cells.[34] Images obtained by confocal microscopy of samples incubated for 24 h with PPPs, and stained with the cell tracker CMTPX, showed a higher uptake of FA-targeted semiconducting polymeric patchy particles (SPPPs) than untargeted particles (Figure 7). Most of the particle's population is located in the cytoplasm of the cell, although some particles are found in the nucleus of the cell.

In order to demonstrate the enhancement of the natural PA signal of patchy polymeric particles by modifying their internal structure, we synthesized particles that envelope poly[2,6-(4,4-bis(2- ethylhexyl)-4*H*-cyclopenta[2,1-*b*;3,4-*b*-*alt*-4,7 (2,1,3benzothiadiazole), a semiconducting polymer that emits a high PA signal. These new synthesized particles of 551 nm in average size are named as semiconducting polymeric patchy particles (SPPPs). The semiconducting polymer enhances substantially the PA signal of PLGA patchy particles and such, the PA signal of SPPPs is similar to that emitted by GNRs at 0.05 and 0.1 mg/mL as shown in Figure 8. The PA signal of the SPPPs is approximately 2 orders of magnitude lower than that of GNRs at 0.5 mg/mL.

Cross-sections of the SPPPs reveal that these particles are hollow (Figure 9). Therefore, there is a possibility that the semiconducting polymer might be forming an inner lining in the particle's core. Further experiments will be required to test this hypothesis.

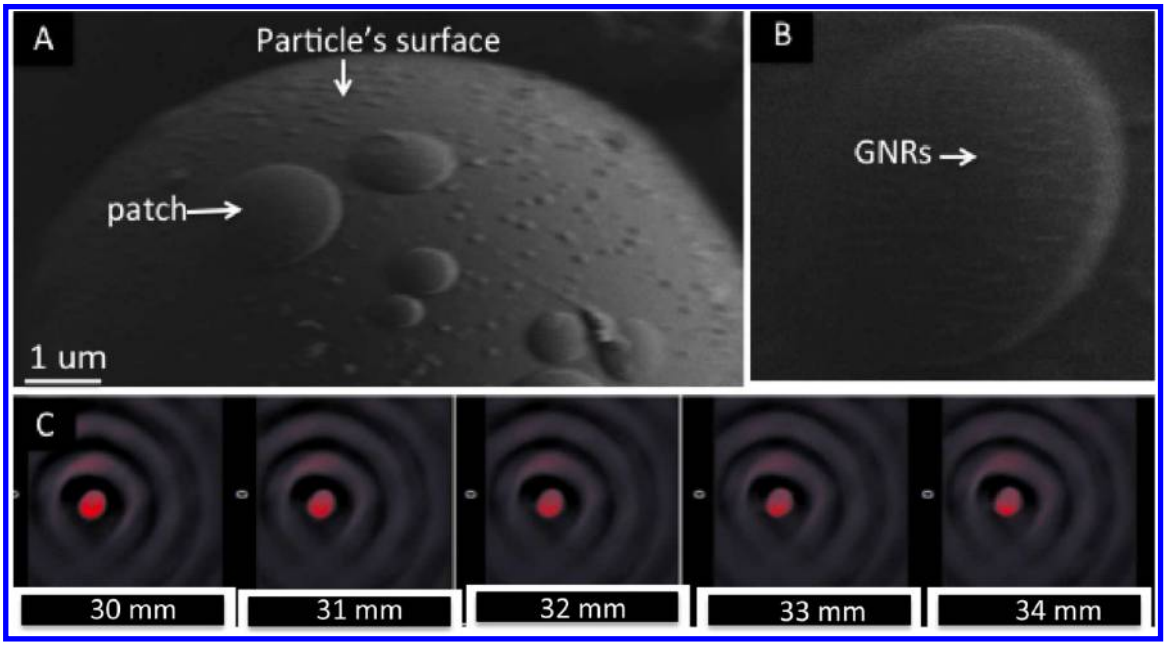

Figure 6. Multipatch particle functionalized with GNRs. (A) Both the particle's core and patch were functionalized with GNRs. (B) Close-up of the particle's patch showing the presence of GNRs. (C) MSOT signal of multipatch particles. Spectral unmixing using the particle's optical absorbance spectrum highlights areas of high photoacoustic signal produced by the multipatch particles in the phantom, shown in red.

DOI: 10.1021/acs.langmuir.6b02177
Langmuir 2016, 32, 7929−7942

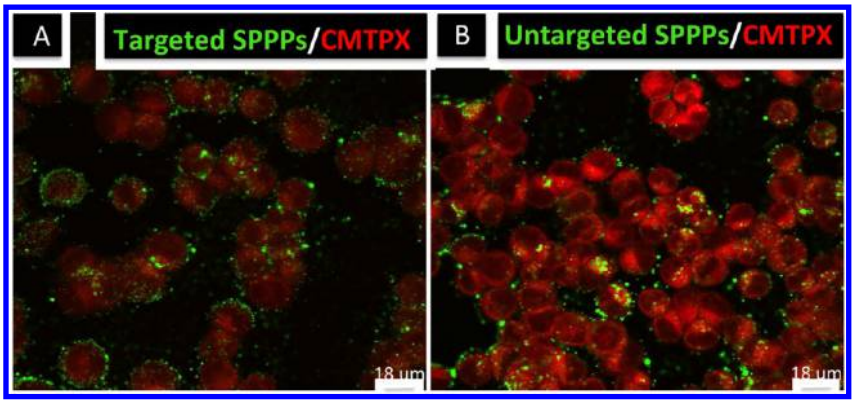

Figure 7. Cellular uptake of PPPs by KB3-1 ovarian cancer cells. (A) Cellular uptake of FA-targeted PPPs. (B) Cellular uptake of untargeted PPPs. FA-targeted particles show higher cellular uptake than untargeted particles. Particles are localized mostly in the cytoplasm of the cell.

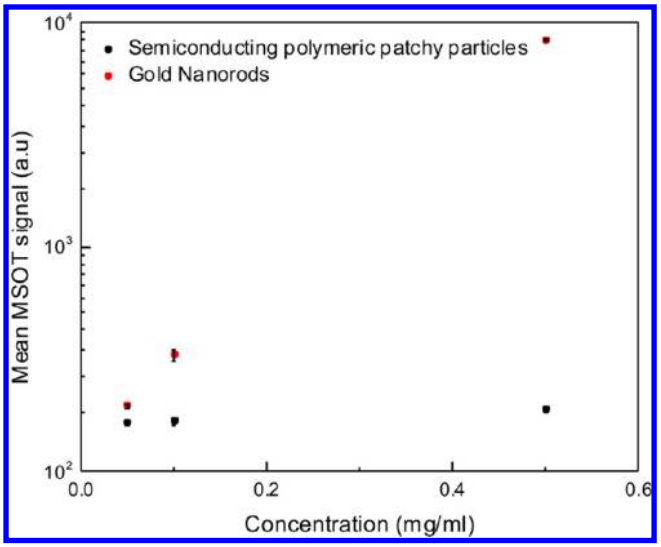

Figure 8. Comparison of the photoacoustic signal of GNRs and SPPPs at different concentrations. The photoacoustic signal of GNRs is approximately 2 orders of magnitude higher than that of SPPPs at 0.5 mg/mL, but it is very similar at 0.1 and 0.05 mg/mL concentrations.

The targeting ability of folic acid-targeted and untargeted SPPPs was assessed in KB3-1 ovarian cancer cells by flow cytometry and confocal microscopy. The histograms of cells incubated for 24 h with particles, with an average size of 551 nm, show a high number of FA-targeted SPPPs taken by KB3-1 cells compared to that of untargeted SPPPs (Figure 10A–C). This result correlated very well with the confocal studies performed previously (Figure 7), which showed the avidly cellular uptake of FA-targeted particles compared with that of untargeted particles after 24 h of incubation. Figure 10D shows Z-stack images of FA-targeted SPPPs. These confocal images reveal that SPPPs are localized mainly in the cytoplasm of the cells.

The PA effect of targeted SPPPs was analyzed *in vivo* using tumor-bearing mice induced with KB3-1 ovarian cancer cells. FA-targeted SPPPs were injected intravenously via tail injection using 200 μL at 0.5 mg/mL concentration. Mice were scanned with a multispectral optical tomography (MSOT) machine 24 h postinjection. The results obtained from the MSOT showed that folic acid-targeted SPPPs are able to target the ovarian cancer tumor and induce a PA signal at deep regions in the tumor (e.g., 23 mm) (Figure 11). Thus, both *in vitro* and *in vivo* studies demonstrate the use of SPPPs in the biomedical imaging field. Further animal studies with particles of small size (e.g., 200 nm) could enhance tumor targeting and therefore, it is expected to observe a higher PA signal in the tumor.

CONCLUSIONS

Using an integrative experimental and computational approach, we elucidated the self-assembly process involved in the formation of PLGA particles with single and multiple patches which are formed by the unique arrangement of LPFGs. We found that, in the presence of a high shear stress force, particles with single patches and with a hollow core are formed because the shear stress force overcomes the van der Waals interaction between DSPE and PLGA. Particles with multiple patches and solid core are formed when the shear stress is low, and therefore, the van der Waals interaction between DSPE and PLGA is strong. Thus, the shear stress determines both the internal and external morphology of PLGA particles as well as their unique natural PA properties. Additionally, MD revealed the formation of a lipid bilayer on the particle's surface as we initially hypothesized.

The high characterization of patchy polymeric particles using both experimental and computational approaches allows us to control several important external and internal features of our particles such as the thickness of the particle's shell, the nature of the particle's core (solid or hollow core by synthesizing the particles at 2000 or 4000 rpm, respectively), single or multiple patches, the incorporation of diverse payloads such as chemotherapeutics or semiconducting polymers depending on the intended medical usage. If the particle's shell is very thin, most likely the release of the drug will be faster than that in particles with a thick shell because, in the former, the drug is not embedded in the polymer matrix but rather confined by it, and the only PLGA available, it is the one forming the particle's shell which has a specific thickness. In microparticles with a solid core, the drug release of the payload will be slower than in hollow particles because the drug is embedded in the polymer matrix and it will take more time for the polymer to degrade via the bulk erosion process. Thus, we can control the drug release profile of patchy particles by tuning the shear stress that the polymer solution undergoes during the emulsification step in the particle synthesis. Equally important, these fundamental experimental and computational studies help us achieve batch control and scalability by identifying the magnitude of the shear stress that is needed to obtain particles with single or multiple patches as the patch is the most distinctive feature of the particles. Consequently, the understanding of the kinetics of the

DOI: 10.1021/acs.langmuir.6b02177
Langmuir 2016, 32, 7929–7942

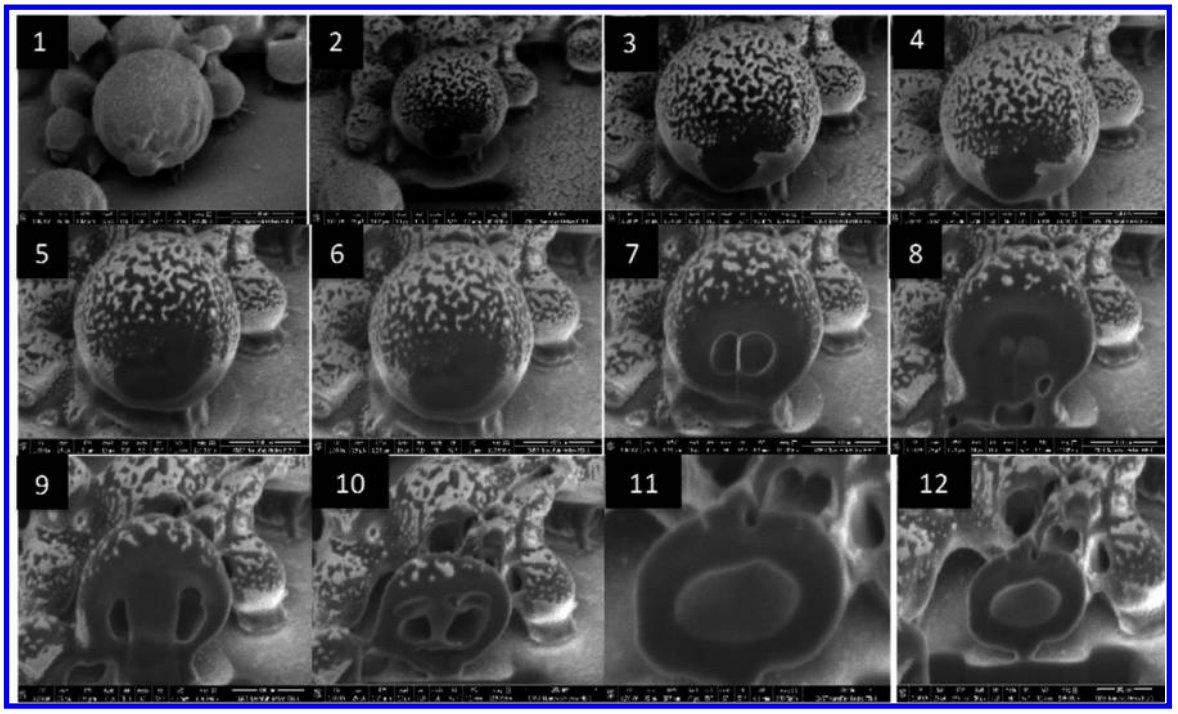

Figure 9. Cross-sections of SPPPs. The cross-sections show that SPPPs are hollow. This finding might suggest that the semiconducting polymer might form the inner lining of the particle's shell. The cross-sections were taken with a step size of 100 nm.

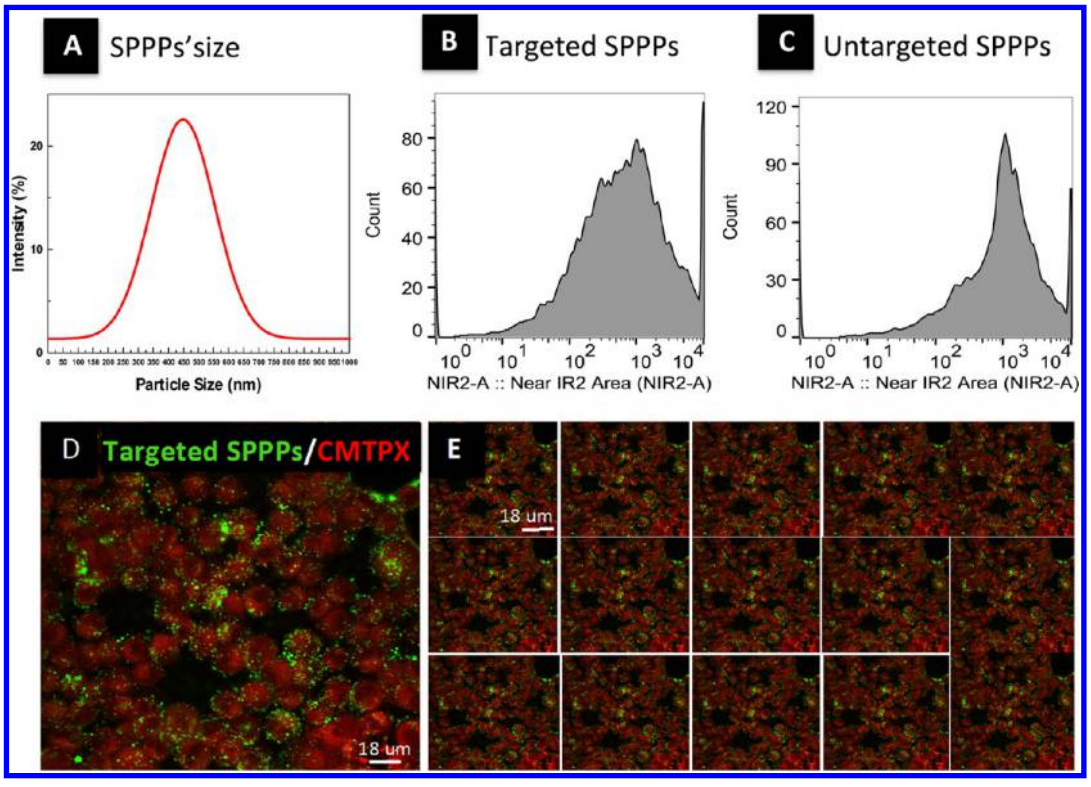

Figure 10. Cellular uptake of FA-targeted and untargeted SPPPs by KB3-1 ovarian cancer cells after 24 h of incubation. (A) FA-targeted SPPPs with an average size of 551 nm. (B) Targeting ability of FA-targeted SPPPs. (C) Targeting ability of untargeted SPPPs. (D) Z-stack images of the cellular uptake of FA-targeted SPPPs by KB3-1 cells. The confocal pictures show that FA-targeted SPPPs have higher cellular uptake than that of untargeted SPPPs. The SPPPs are mostly in the cytoplasm of the cell, although some of the particles are in the cells' nucleus. The Z-stack shows that SPPPs are inside the cells and not on the particle's surface. The Z-stack was taken with a step size of 0.10 μm.

self-assembly of PLGA and LPFGs will help accelerate the medical translation process of PLGA particles. Furthermore, it is important to mention that the novel MD on the PLGA-DSPE-PEG-NH_2 system will be of great utility for the scientific community as this polymer system is commonly used in the synthesis of many nanotherapeutics. Moreover, additional MD

DOI: 10.1021/acs.langmuir.6b02177
Langmuir 2016, 32, 7929−7942

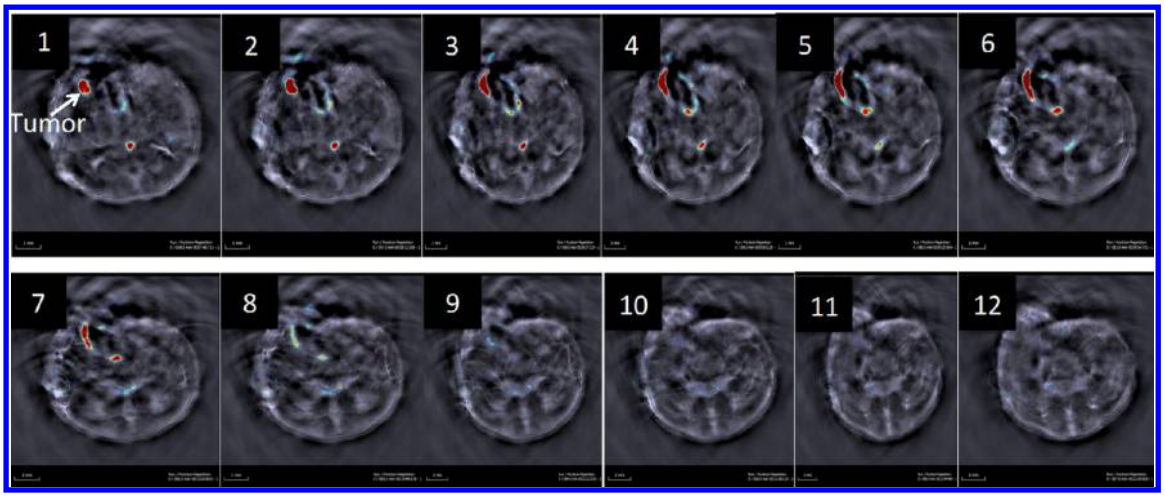

Figure 11. *In vivo* PA performance of SPPPs. MSOT images of SPPPs in tumor site after 24 h postinjection. Multispectral processing of the MSOT data in tissue identifies the presence of the SPPPs within the tumor region, as indicated by the colored regions.

simulations are needed to elucidate the arrangement of the LPFGs in the particle's patch. Additionally, both the *in vitro* and *in vivo* experiments reported in this work show not only the feasibility of the biomedical applications of patchy polymeric nanoparticles but also the potential to advance the biomedical imaging field by developing highly characterized PA molecules probes.

EXPERIMENTAL SECTION

Synthesis of Lipid–Polymeric Patchy Particles. Particles with single and multiple patches were prepared by a single-emulsion method as reported in Salvador-Morales et al. and Rasheed et al.[14,25] Briefly, the aqueous phase of the mixture was prepared by dissolving DSPE-PEG(2000) amine 1,2-distearoyl-*sn*-glycero-3-phosphoethanolamine-*N*-[amino(poly(ethylene glycol))-2000 (DSPE-PEG-NH_2) or DSPE-PEG(2000) maleimide 1,2-distearoyl-*sn*-glycero-3-phosphoethanolamine-*N*-[maleimide(poly(ethylene glycol))-2000 (DSPE-PEG-MAL) in 4% ethanol to a concentration of 1 mg/mL. To this solution, 6 mL of 4% ethanol was added and the solution was homogenized at 1000 rpm for 15 s. A 4 mL aliquot of PLGA solution (15 mg/mL in ethyl acetate) was immediately added to the aqueous phase. The mixture was homogenized at 2000 or 4000 rpm for 1 min using a L5M-A high shear mixer and 5/8 in. tubular mixing assembly. A 50 mL aliquot of deionized water was added dropwise to the emulsified mixture, and the volatile solvent was allowed to evaporate overnight. Particles were centrifuged at 2000 rpm for 10 min using Millipore Amicon Ultra centrifugal filter units with a MWCO of 100 kDa to remove the remaining solvent completely and washed three times with deionized water. Subsequently, Particles were examined with a FE-SEM (Zeiss) operating at 1.00 kV accelerating voltage to visualize the particle's surface. The aqueous phase of particles with multiple patches was prepared with 1 mL of DSPE-PEG-NH_2 and 1 mL of DSPE-PEG-MAL. DSPE-PEG-NH_2 was labeled with Alexa 594 (5 μg) before being mixed with DSPE-PEG-MAL.

Cross-Sections of Particles. Patchy polymeric particles and semiconducting polymeric patchy particles were cross-sectioned using a FEI focused ion beam with a gallium ion source operated at 1 kV and an SE detector and at different magnifications. Both types of particles were previously coated with gold–palladium alloy to protect particles from the ion beam. The step size for the patchy polymeric particles was 500 nm while, for the semiconducting polymeric nanoparticles, 100 nm.

Computational Fluid Dynamics Simulations. In order to demonstrate the dependence of the fluid shear stress on the size of the gap between the inner diameter of the homogenizer tubular assembly's workhead and the rotor shaft, computational fluid dynamics (CFD) simulations were carried out with a gap size of 0.137 mm. The numerical solutions of 3D incompressible Navier–Stokes equations were obtained with an edge-based finite element solver developed in-house. Unstructured grids composed of tetrahedral elements were generated and locally refined near the inner wall to obtain at least two points within the gap. The resulting mesh had approximately 3 million elements. We modeled the rotating piece using immersed boundary methods based on unstructured grids. The rotor shaft was set in rigid-body rotation around its axis at 4000 and 2000 rpm. No-slip boundary conditions were applied at all body surfaces, including the rotating rotor shaft. The polymer fluid density was set to 1.0 g/cm^3 and the viscosity to 0.031 dyn s/cm^2. The viscosity of the polymer solution was measured using a MCR702 rheometer (Anton Paar GmbH) with a double-gap configuration. We used an explicit three-stage Runge–Kutta scheme with CFL = 0.6 and a maximum time step of 5×10^{-5} to advance the flow solution. All simulations were carried out in parallel on shared memory computers using OpenMP and were run on 16 processors. We saved results at 1.5×10^{-4} s intervals and created animations of the wall shear stress in the gap region.

Molecular Dynamics Simulations. *Full-Atomistic Molecular Dynamics Simulation.* The full-atom structures for PLGA and DSPE-PEG polymers were built, by dividing each one into parts. In the case of PLGA, two monomers (lactic acid and glycolic acid) were formed and, later, replicated at random, making a total of 419 lactic acids (76%) and 131 glycolic acids (24%) monomers for a single chain of PLGA. Lactic acid and glycolic acid monomers were parametrized using CHARMM general force field (CGenff)[35] and PARAMCHEM platform,[36,37] as previously described for poly(ethylene oxide) polymers.[38] Meanwhile, in the case of DSPE-PEG, the molecule was divided into a single monomer of DSPE and 45 monomers of PEG. DSPE section was parametrized using CHARMM36 force field of lipids,[39] while PEG parameters were obtained from ethers force field CHARMM35.[40]

First, to obtain a compacted structure, a molecular dynamics simulation in vacuum for DSPE-PEG was carried out, using the canonical ensemble. Once a compact structure was obtained, a single PLGA chain and four DSPE-PEG polymers were placed into a TIP3P water box with a salt concentration of 0.15 M.[41] Then, an energy minimization phase using conjugate gradients algorithm under NAMD software was carried out for each system.[42] Later, the system was equilibrated by molecular dynamics in the isobaric–isothermal ensemble, under periodic boundary conditions, at 1 bar and 310 K, during 50 ns. All systems were built using VMD software.[43] Langevin dynamics, with a damping coefficient of 1 ps and the Nosé–Hoover Langevin piston method was applied to keep constant the temperature and pressure.[44] RATTLE algorithm was applied to constrain all hydrogen bonds.[45] Long-range electrostatic interactions were calculated using the particle mesh Ewald (PME) algorithm, and short-range,

DOI: 10.1021/acs.langmuir.6b02177
Langmuir 2016, 32, 7929–7942

van der Waals forces were estimated within a cutoff of 10 Å.[46] Equations of motion were integrated using a time step of 2 fs.

Coarse-Grained Molecular Simulations. To study the self-assembly and interaction of several DSPE-PEG molecules with the nanoparticle in a bigger system, we may require exploring longer time scales, prohibitive for full-atomistic simulations. In these cases, coarse-grained models, which consider a smaller number of particles, become useful. The MARTINI force field (CG) is a coarse-grained model adopted for biomolecular systems.[47] This model has four interaction "bead" types: polar (P), apolar (C), nonpolar (N), and charged (Q), used to simulate lipids, proteins, and carbohydrates. These types are subclassified into 18 types of interaction according to hydrogen-bonding capabilities and polarity. This force field has been parametrized based on the reproduction of partitioning free energies between polar and nonpolar phases. A coarse-grained model for PEG was developed by Lee et al., using distributions of bonds, angles, and dihedrals from CHARMM all-atom FF.[48] Later, a model for PEGylated lipid (DPPE-PEG45) was developed on the basis of this first model.[49] Parameters of these models are available in MARTINI Web site (https://www.md.chem.rug.nl) and were adapted to this work for the molecular structures of DSPE-PEG.

Few articles have been written on the development of a coarse-grained model for PLGA or PLA.[50,51] Considering that, in the present coarse-grained study, PLGA polymers are treated as a rigid block, and since we are more interested in the study of the self-assembly of DSPE-PEG polymers on the surface of this block, we took a rough strategy to deal with the absence of MARTINI parameters for PLGA. In this manner, we assigned two beads, P1, and P3, to model lactic acid and glycolic acid monomers, respectively, in the PLGA chain. The assignment was made on the basis of choosing the most similar bead, taking into account the method suggested by Marrink et al.[47] It is important to note that a refined model may be required to evaluate different parameters of PLGA−PLGA interaction at the coarse-grained level. The structures of DSPE-PEG and PLGA beads are depicted in Figure S2 (see Supporting Information).

Full-atomistic simulations of polymers in explicit water were transformed to coarse-grained resolution using the mapping described above. The distribution of equilibrium values and force constants for bonded interactions were measured along mapped-to-CG-atomistic simulations, as suggested by Martini developers.[52] The radius of gyration was obtained from CG models and compared with full-atom models, as a way to validate the models.

A PLGA nanoparticle, composed by 19800 chains, containing 4752 molecules of glycolic acid and 15045 of lactic acid, was placed in the bottom of a nonpolarized MARTINI water box with dimensions 146 × 143 × 385 $Å^3$. To study how PEGylated lipids are spread out over the surface of the PLGA nanoparticle, 360 monomers of DSPE-PEG were placed at random above of the nanoparticle. To avoid the interaction of the PLGA nanoparticle with the upper part of the box due to the periodic boundary conditions, and in this way, simulate the collapse of DSPE- PEG into the nanoparticle, a graphene film was placed at the bottom of the box. The film was kept restrained with a harmonic constant of 1000 kJ mol^{-1} nm^{-1}. Molecular dynamics simulations were performed using GROMACS package (version 5.0.3).[53] The energy minimization stage was conducted employing the steepest descent method, with a force tolerance of 10 kJ mol^{-1} nm^{-1}, until reaching convergence. The equilibration step was carried out at canonical ensemble, at room temperature, using the Berendsen thermostat, during 240 ns. From this point, molecular dynamics simulation at 10 bar was performed, under *NPT* ensemble, to simulate the application of an external force, such as in the centrifugation process employed in the experiments. To this end, Berendsen barostat was applied during about 1 μs.[54] All simulations were done using short-range electrostatics and Lennard-Jones potentials, which were shifted to zero from 0.0 and 0.9 nm, respectively, to the cutoff distance (1.2 nm), using the standard shift function in GROMACS.[55] Long-range electrostatics was taken into account using PME summation.[46] An integration time step of 10 fs was considered.

Differential Scanning Calorimetry Studies. Thermal analyzes of the materials were run on a TA Instruments T100 differential scanning calorimeter from −90 to 90 °C, at a rate of 10 °C/min. Patchy particles with single and multiple patches were synthesized as described in the particle's synthesis section. For these thermal studies, particles with single patches were prepared only with DSPE-PEG-NH_2 and labeled with Alexa 647 (5 μg). Samples were lyophilized before thermal scans. Enthalpies of transition were calculated by normalizing the transition peak of the thermogram and integrating with Origin software.

Photoacoustic Measurements. The phantom was created by boiling 1.0 g of agar in 50 mL of deionized water. Also, 2.5 mL of intralipid was added in order to mimic the light scattering properties of the tissue. The solution was poured into a cylindrical mold with a solid rod suspended in the center, and then the agar was allowed to set. The rod created a long bore along the axis of the cylindrical phantom, which later will serve as the sample holder. For PA imaging and measurement of the samples, a 200 μL of solution was prepared. It was then loaded into a plastic straw, and hot glue was used to seal both ends. This was placed in the previously created bore in the center of the agar phantom. Photoacoustic measurements of the phantom were then obtained with the inVision-256TF multispectral optoacoustic tomography system (iThera Medical, Munich, Germany). The photoacoustic signals were measured at 700 nm wavelength and averaging four frames. Axial scans of the phantom were taken slice by slice in 1 mm increments. These imaging conditions were found to be optimal for imaging the phantom and getting reproducible data from them. The obtained data were further processed by feeding in the absorbance spectrum of the sample, obtained earlier using a spectrophotometer, to spatially localize the PA source emitted by the sample at 700 nm wavelength. The photoacoustic signal was analyzed by drawing an elliptical region of interest (ROI) around the area of the straw in each slice that was located inside the phantom. The mean signal within that ROI was recorded for each sample at the same slice.

Functionalization of Multipatch Particles with Gold Nanorods. Multipatch particles with DSPE-PEG-maleimide were synthesized as described above and functionalized with gold nanorods functionalized with thiol groups. A 2 mg amount of multipatch particles was suspended in deionized water (diH_2O) and 30 μL of gold nanorods (2.6 mg/mL) were added to the reaction beaker. The mixture was incubated for 2 h in stirring conditions at room temperature. After the incubation step, the sample was washed three times with diH_2O and filtered to remove unbound gold nanorods. After the functionalization process, a sulfur bond is formed between the gold nanorods and multipatch particles. Gold nanorods were purchased from NanoPartz Inc. The diameter and length of the gold nanorods are 10 and 41 nm, respectively, according to the certificate of analysis. Functionalized microparticles with gold nanorods were examined with SEM operated at 1 kV. The PA measurements were taken as described in Photoacoustic Measurements.

Conjugation of Folic Acid to DSPE-PEG-NH_2. A 0.1 g amount of folic acid was dissolved in 4 mL of anhydrous dimethyl sulfoxide (DMSO) and 50 μL of triethylamine. The mixture was stirred in dark and inert conditions overnight. Subsequently, 50 mg of *N*,*N*′-dicyclohexylcarbodiimide (DCC) and 28 mg of *N*-hydroxysuccinimide (NHS) were added to the reaction and stirred for 18 h. Next, the side product dicyclohexylurea (DCU) was removed using an Amicon filter with molecular weight of 10 kDa. Activated FA (i.e., FA-NHS) was lyophilized overnight. A 13 mg amount of refined powder of FA-NHS were dissolved in 26 mL of DSPE-PEG-NH_2 and 26 mL of 10× PBS, pH 7.4. Unreactive FA-NHS was removed by filtration. DSPE-PEG-FA was lyophilized for several hours, and an aliquot of it was analyzed with proton nuclear magnetic resonance (NMR) spectroscopy.

Nuclear Magnetic Resonance Analysis of the Conjugation of Folic Acid to DSPE-PEG-NH_2. We utilized ^{1}H NMR spectroscopy to verify the conjugation of FA to DSPE-PEG-NH_2. A 30 mg amount of DSPE-PEG-NH_2 or DSPE-PEG-FA was dissolved in 0.8 mL of diH_2O and transferred to a glass NMR tube. The samples were analyzed by ^{1}H NMR spectroscopy. The ^{1}H NMR spectra were taken with a 400 MHz, Bruker DRX 400 instrument. The spectra were obtained within a few days of sample preparation with an acquisition time of 2.2675955

DOI: 10.1021/acs.langmuir.6b02177
Langmuir 2016, 32, 7929−7942

s and relaxation delay of −2 s. (See Figure S1 of the Supporting Information to see the NMR spectra.)

Synthesis of Folic Acid-Targeted and Untargeted Polymeric Patchy Particles. Particles were synthesized via the emulsion method described in Rasheed et al.[25] Briefly, the organic phase of the emulsion was formed by PLGA (inherent viscosity, 0.55−0.75 dL/g; 75:25) previously dissolved in ethyl acetate at a concentration of 10 mg/mL. In order to label the particles, 100 μg of NBD−cholesterol (22-(*N*-(7-nitrobenz-2-oxa-1,3-diazol-4-yl)amino)-23,24-bisnor-5-cholen-3β-ol) was added to the oil phase. For folic acid-targeted polymeric particles, the aqueous phase was composed of 15 mL of DSPE-PEG-NH_2 (1 mg/mL in diH_2O), 5 mL of DSPE-PEG-FA (1 mg/mL), and 36 mL of diH_2O. For untargeted particles 15 mL of DSPE-PEG-NH_2 (1 mg/mL) and 41 mL of diH_2O were used. The immiscible mixture was emulsified at 8000 rpm for 4 min using a 1 in. homogenizer's workhead. Subsequently, 300 mL of deionized water was added dropwise to the emulsified particle solution and stirred overnight to evaporate the solvent. Next day, the polymeric particles were filtered with an Amicon filter (100 kDa cutoff). Samples were washed twice in phosphate buffered saline (PBS) and dialyze overnight in PBS.

Synthesis of Folic Acid-Targeted and Untargeted Semiconducting Polymeric Patchy Particles. Particles were synthesized via the emulsion method described in Rasheed et al.[25] Briefly, the organic phase of the emulsion was formed by PLGA (inherent viscosity, 0.55-0.75 dL/g; 75:25) previously dissolved in ethyl acetate at a concentration of 10 mg/mL. A 3 mg amount of poly[2,6-(4,4-bis(2-ethylhexyl)-4*H*-cyclopenta[2,1-*b*;3,4-*b*-*alt* 4,7(2,1,3benzothiadiazole)] (PCPDTBT) was dissolved in 500 μL of chloroform and added to PLGA solution. The aqueous phase was composed of 9 mL of DSPE-PEG-NH_2 (1 mg/mL), 12 mL of sodium dodecyl sulfate (8×10^{-3} M), 3 mL of DSPE-PEG-FA (1 mg/mL), and 36 mL of deionized water. The immiscible mixture was emulsified at 4000 rpm for 4 min using a 1 in. homogenizer's workhead. Subsequently, 300 mL of deionized water was added dropwise to the emulsified particle solution and stirred overnight to evaporate the solvent. Next day, semiconducting polymeric nanoparticles were filtered with an Amicon filter (100 kDa cutoff). Samples were washed twice in PBS and dialyzed overnight in PBS. Untargeted semiconducting polymeric patchy particles were prepared as described above but without DSPE-PEG-FA.

Dynamic Light Scattering Characterization of Semiconducting Polymeric Patchy Particles. The SPPPs were suspended in 1× PBS, pH 7.4. The hydrodynamic diameter (nm) of the SPPPs and their polydispersity index were determined from three repeated experiments using a Dynamic Light Scattering system (Beckman Coulter N5 submicrometer particle size analyzer.

Cellular Uptake of Polymeric Patchy Microparticles and Semiconducting Polymeric Patchy Particles by KB3-1 Ovarian Cancer Cells. KB3-1 cells were provided by Dr. Michael M. Gottesman (NCI, NIH, Bethesda, MD) and cultured in DMEM, catalog no. 11995-065, Thermo Fisher Scientific, prepared with 10% fetal bovine serum, 1% penicillin streptomycin (ref 15140-122), and 0.5% L-glutamine (ref 25030-081; Gibco). This culture medium is referred to as complete medium. Next, 8×10^4 cells/well were plated on glass coverslips in complete medium of a 24-well plate and incubated for 24 h. After the incubation period, cells were washed three times with sterile PBS. Then, 500 μL of labeled folic acid-targeted and untargeted particles and semiconducting polymeric patchy particles at 0.5 mg/mL in complete medium were added to each well and incubated for 24 h. After the incubation step, cells were washed 3 times with sterile PBS and incubated at 37 °C for 30 min with 500 μL of complete medium containing 1 μM CMTPX cell tracker (catalog no. C34552, Life Sciences, USA). The CMTPX is a fluorescence probe that allows one to stain the cytoplasm and part of the cell membrane. Subsequently, cells were washed once with PBS and fixed with 4% paraformaldehyde for 30 min at room temperature followed by three washed with PBS. The glass coverslips were mounted on glass and mounting medium, and examined with a confocal microscope (Nicon C1 plus), 60× oil objective, medium pinhole, and lasers at 488 and 561 nm. Z-stack confocal pictures were taken from each sample. The step size was 0.10 μm, 15 steps, and medium pinhole.

Assessment of the Targeting Ability of DSPE-PEG-Folic Acid in KB3-1 Cells. To assess the effectiveness of DSPE-PEG-FA in ovarian cancer, we conducted flow cytometry studies. For 24 h, 8×10^4 cells were cultured in a 96-well plate at 37 °C and 5% CO_2 in complete medium. Subsequently, FA-targeted and untargeted semiconducting polymeric patchy particles at 0.5 mg/mL prepared in complete medium were added to cells and incubated for 24 h at 37 °C and 5% CO_2. After 24 h, the old medium was removed and cells were trypsinized to be detached from the bottom of the well. Samples were centrifuged at 10000 rpm for 20 min in a microcentrifuge and supernatant was removed followed by two washes with PBS. After the second wash, samples were fixed with 4% paraformaldehyde and incubated at room temperature for 20 min. The 4% paraformaldehyde solution was removed, and samples were suspended in fluorescence-activated cell sorting (FACS) buffer prepared with PBS and containing 1% (v/v) fetal bovine serum. Subsequently, FACS measurements were recorded with a GUAVA−Millipore instrument. The FACS data were analyzed with the FlowJo single-cell analysis software.

Animal Studies. All animal experimental procedures were reviewed and approved by the Institutional Animal Care and Use Committee (IACUC) at Virginia Commonwealth University (VCU). Female nude mice, aged between 6 and 8 weeks, were obtained from Envigo Research Models and Services, Indianapolis, IN, USA, caged in groups of five or fewer, and food and water was provided ad libitum. Animals were anesthetized with 2% isoflurane in oxygen during tumor implantation and imaging. All efforts were made to minimize pain and suffering. Animals were euthanized by using controlled release of CO_2 from a cylinder into a chamber that allowed good visibility of the animals and was large enough to avoid crowding. All the live animal experiments were performed according to the policies and guidelines of the IACUC at VCU.

In Vivo Assessment of the Folic Acid-Targeted Semiconducting Polymeric Particles' PA Performance. KB3-1 ovarian cancer cells in PBS and matrigel (1:1) were implanted subcutaneously in the flank. Imaging experiments were conducted when the tumors reached a size of ∼150 mm^3. Animals were fed with folate-free diet (Harlan Teklad, USA) for a total of 5 weeks, starting from a period before tumor implantation, while the tumors were growing, and during the experiments. Folic acid-targeted semiconducting polymeric patchy particles were injected via tail injection at 0.5 mg/mL, and photoacoustic images were acquired using the inVision-256TF multispectral optoacoustic tomography system (iThera Medical, Stamford, CT, USA). Whole-body live animal imaging was performed at 24 h postinjection, with the field of view encompassing the entire tumor, and transverse slices were imaged in 0.5 mm steps, at all wavelengths from 680 to 980 at 10 nm increments, using eight averages per wavelength. A linear regression reconstruction method was used to process the raw photoacoustic data. The optical absorbance spectrum of the patchy particles, measured earlier using a spectrophotometer, was fed into the reconstruction parameters and multispectral unmixing was performed in postprocessing of the photoacoustic signal produced by the patchy particles in the living animal.

■ ASSOCIATED CONTENT

Supporting Information

The Supporting Information is available free of charge on the ACS Publications website at DOI: 10.1021/acs.langmuir.6b02177.

Movie of the Computational Fluid Dynamics Simulations of the homogenizer workhead and rotor-shaft used in the particle's synthesis. The CFD show the low and high shear stress generated when particles are synthesized at 2000 and 4000 rpm, respectively (MPG)

DOI: 10.1021/acs.langmuir.6b02177
Langmuir 2016, 32, 7929−7942

Movie of the coarse-grained simulation of the self-assembly of DSPE-PEGpolymer into the surface of PLGA block (AVI)

Movie of the Molecular Dynamics Simulations showing the self-assembly of DSPE-PEG polymer into the surface of PLGA block (AVI)

NMR spectra for DSPE-PEG-FA and -NH_2, and full-atom structures for DSPE-PEG and PLGA polymers (PDF)

AUTHOR INFORMATION

Corresponding Author

*E-mail: csalvado@gmu.edu.

Notes

The authors declare no competing financial interest.

ACKNOWLEDGMENTS

This research was supported by NSF Grant No. CBET-1348112 and GMU Seed Grant No. 130978 obtained by C.S.-M. and C.S.-M.−J. Cebral−J.Z., respectively. Research was performed in part at the NIST Center for Nanoscale Science and Technology. We thank the NIST Center for Nanoscale Science and Technology for the use of the focused ion beam instrument and Joshua Schumacher and Kerry Siebein for their assistance in helping to take the patchy polymeric particles' cross-sections. V.M.-M. thanks CONICYT for a Ph.D. Scholarship and CONICYT + PAI/"Concurso Nacional Tesis de Doctorado en la Empresa" 2014 (Grant No. 781413007). F.G-N., V.M-M., I.A.-D., and J. Cebral are grateful for the support of Fraunhofer Chile Research, Innova-Chile CORFO (Grant No. FCR-CSB 09CEII-6991), RED CYTED 214RT0482, and Anillo Científico ACT1107. C.V. acknowledges the support of the Center for the Development of Nanoscience and Nanotechnology (CEDENNA)—BASAL Grant FB0807—and FONDECYT Grant No. 1161438 CONICYT-Chile. We thank Dr. Michael M. Gottesman (NCI, NIH, Bethesda, MD, USA) for providing the KB-3-1 cells.

REFERENCES

(1) Glotzer, S. C.; Solomon, M. J. Anisotropy of building blocks and their assembly into complex structures. *Nat. Mater.* **2007**, *6*, 557−562.

(2) Champion, J. A.; Katare, Y. K.; Mitragotri, S. Particle shape: A new design parameter for micro- and nanoscale drug delivery carriers. *J. Controlled Release* **2007**, *121*, 3−9.

(3) Cui, J. Q.; Kretzschmar, I. Surface-anisotropic polystyrene spheres by electroless deposition. *Langmuir* **2006**, *22*, 8281−8284.

(4) Pawar, A. B.; Kretzschmar, I. Fabrication, Assembly, and Application of Patchy Particles. *Macromol. Rapid Commun.* **2010**, *31*, 150−168.

(5) Hong, L.; Jiang, S.; Granick, S. Simple method to produce Janus colloidal particles in large quantity. *Langmuir* **2006**, *22*, 9495−9499.

(6) Roh, K. H.; Martin, D. C.; Lahann, J. Biphasic Janus particles with nanoscale anisotropy. *Nat. Mater.* **2005**, *4*, 759−763.

(7) Roh, K. H.; Martin, D. C.; Lahann, J. Triphasic nanocolloids. *J. Am. Chem. Soc.* **2006**, *128*, 6796−6797.

(8) Pawar, A. B.; Kretzschmar, I. Patchy particles by glancing angle deposition. *Langmuir* **2008**, *24*, 355−358.

(9) Pawar, A. B.; Kretzschmar, I. Multifunctional patchy particles by glancing angle deposition. *Langmuir* **2009**, *25*, 9057−9063.

(10) Yake, A. M.; Snyder, C. E.; Velegol, D. Site-specific functionalization on individual colloids: size control, stability, and multilayers. *Langmuir* **2007**, *23*, 9069−9075.

(11) Snyder, C. E.; Yake, A. M.; Feick, J. D.; Velegol, D. Nanoscale functionalization and site-specific assembly of colloids by particle lithography. *Langmuir* **2005**, *21*, 4813−4815.

(12) Romanski, F. S.; Winkler, J. S.; Riccobene, R. C.; Tomassone, M. S. Production and characterization of anisotropic particles from biodegradable materials. *Langmuir* **2012**, *28*, 3756−3765.

(13) Kim, M. R.; Lee, S.; Park, J. K.; Cho, K. Y. Golf ball-shaped PLGA microparticles with internal pores fabricated by simple O/W emulsion. *Chem. Commun.* **2010**, *46*, 7433−7435.

(14) Salvador-Morales, C.; Valencia, P. M.; Gao, W.; Karnik, R.; Farokhzad, O. C. Spontaneous formation of heterogeneous patches on polymer-lipid core-shell particle surfaces during self-assembly. *Small* **2013**, *9*, 511−517.

(15) Xiang, B.; Dong, D. W.; Shi, N. Q.; Gao, W.; Yang, Z. Z.; Cui, Y.; Cao, D. Y.; Qi, X. R. PSA-responsive and PSMA-mediated multifunctional liposomes for targeted therapy of prostate cancer. *Biomaterials* **2013**, *34*, 6976−6991.

(16) Hu, R.; Wang, Y. C.; Liu, X.; Lin, G. M.; Tan, C. H.; Law, W. C.; Roy, I.; Yong, K. T. Rational design of multimodal and multifunctional InP quantum dot nanoprobes for cancer: in vitro and in vivo applications. *RSC Adv.* **2013**, *3*, 8495−8503.

(17) Feng, G.; Ding, D.; Li, K.; Liu, J.; Liu, B. Reversible photoswitching conjugated polymer nanoparticles for cell and ex vivo tumor imaging. *Nanoscale* **2014**, *6*, 4141−4147.

(18) Wang, A. T.; Liang, D. S.; Liu, Y. J.; Qi, X. R. Roles of ligand and TPGS of micelles in regulating internalization, penetration and accumulation against sensitive or resistant tumor and therapy for multidrug resistant tumors. *Biomaterials* **2015**, *53*, 160−172.

(19) Doolittle, E.; Peiris, P. M.; Doron, G.; Goldberg, A.; Tucci, S.; Rao, S.; Shah, S.; Sylvestre, M.; Govender, P.; Turan, O.; Lee, Z.; Schiemann, W. P.; Karathanasis, E. Spatiotemporal Targeting of a Dual-Ligand Nanoparticle to Cancer Metastasis. *ACS Nano* **2015**, *9*, 8012−8021.

(20) Li, Y.; Wu, H.; Jia, M.; Cui, F.; Lin, J.; Yang, X.; Wang, Y.; Dai, L.; Hou, Z. Therapeutic effect of folate-targeted and PEGylated phytosomes loaded with a mitomycin C-soybean phosphatidyhlcholine complex. *Mol. Pharmaceutics* **2014**, *11*, 3017−3026.

(21) Wang, L.; Wang, C.; Jiao, J.; Su, Y.; Cheng, X.; Huang, Z.; Liu, X.; Deng, Y. Tolerance-like innate immunity and spleen injury: A novel discovery via the weekly administrations and consecutive injections of PEGylated emulsions. *Int. J. Nanomed.* **2014**, *9*, 3645−3657.

(22) Liu, D.; Liu, F.; Liu, Z.; Wang, L.; Zhang, N. Tumor specific delivery and therapy by double-targeted nanostructured lipid carriers with anti-VEGFR-2 antibody. *Mol. Pharmaceutics* **2011**, *8*, 2291−2301.

(23) Wen, X.; Wang, K.; Zhao, Z.; Zhang, Y.; Sun, T.; Zhang, F.; Wu, J.; Fu, Y.; Du, Y.; Zhang, L.; Sun, Y.; Liu, Y.; Ma, K.; Liu, H.; Song, Y. Brain-targeted delivery of trans-activating transcriptor-conjugated magnetic PLGA/lipid nanoparticles. *PLoS One* **2014**, *9*, e106652.

(24) Kastantin, M.; Ananthanarayanan, B.; Karmali, P.; Ruoslahti, E.; Tirrell, M. Effect of the lipid chain melting transition on the stability of DSPE-PEG(2000) micelles. *Langmuir* **2009**, *25*, 7279−7286.

(25) Rasheed, N.; Khorasani, A. A.; Cebral, J.; Mut, F.; Lohner, R.; Salvador-Morales, C. Mechanisms Involved in the Formation of Biocompatible Lipid Polymeric Hollow Patchy Particles. *Langmuir* **2015**, *31*, 6639−6648.

(26) Wang, Y.; Guo, B. H.; Wan, X.; Xu, J.; Wang, X.; Zhang, Y. P. Janu-like polymer particles prepared via internal phase separation from emulsified polymer/oil droplets. *Polymer* **2009**, *50*, 3361−3369.

(27) Rosca, I. D.; Watari, F.; Uo, M. Microparticle formation and its mechanism in single and double emulsion solvent evaporation. *J. Controlled Release* **2004**, *99*, 271−280.

(28) Pekarek, K. J.; Jacob, J. S.; Mathiowitz, E. Double-walled polymer microspheres for controlled drug release. *Nature* **1994**, *367*, 258−260.

(29) Kraft, D. J.; Hilhorst, J.; Heinen, M. P.; Hoogenraad, M. J.; Luigjes, B.; Kegel, W. K. Patchy polymer colloids with tunable anisotropic dimensions. *J. Phys. Chem. B* **2011**, *115*, 7175−7181.

DOI: 10.1021/acs.langmuir.6b02177
Langmuir 2016, 32, 7929−7942

(30) Ku, K. H.; Kim, Y. J.; Yi, G. R.; Jung, Y. S.; Kim, B. J. Kim. Soft patchy particles of block copolymer from interface-engineered emulsion. *ACS Nano* **2015**, *9*, 11333−11341.
(31) Xiao, C. D.; Shen, X. C.; Tao, L. Modified emulsion solvent evaporation method for fabricating core-shell microspheres. *Int. J. Pharm.* **2013**, *452*, 227−232.
(32) Abulateefeh, S. R.; Alkilany, A. M. Synthesis and Characterization of PLGA Shell Microcapsules Containing Aqueous Cores Prepared by Internal Phase Separation. *AAPS PharmSciTech* **2015**, 1−7.
(33) Li, M.-L.; Wang, J. C.; Schwartz, J. A.; Gill-Sharp, K. L.; Stoica, G.; Wang, L. V. In vivo photoacoustic microscopy of nanoshell extravassation from solid tumor vasculature. *J. Biomed. Opt.* **2009**, *14*, 010507.
(34) Elnakat, H.; Ratnam, M. Role of folate receptor genes in reproduction and related cancers. *Front. Biosci., Landmark Ed.* **2006**, *11*, 506−519.
(35) Vanommeslaeghe, K.; MacKerell, A. D., Jr. Automation of the CHARMM General Force Field (CGenFF) I: bond perception and atom typing. *J. Chem. Inf. Model.* **2012**, *52*, 3144−3154.
(36) Vanommeslaeghe, K.; Raman, E. P.; MacKerell, A. D., Jr. Automation of the CHARMM General Force Field (CGenFF) II: assignment of bonded parameters and partial atomic charges. *J. Chem. Inf. Model.* **2012**, *52*, 3155−3168.
(37) Vorobyov, I.; Anisimov, V. M.; Greene, S.; Venable, R. M.; Moser, A.; Pastor, R. W.; MacKerell, A. D. Additive and Classical Drude Polarizable Force Fields for Linear and Cyclic Ethers. *J. Chem. Theory Comput.* **2007**, *3*, 1120−1133.
(38) Leiva, A.; Fuentes, I.; Bossel, E.; Urzua, M.; Mendez, M.; Pino, M.; Radic, D.; Marquez, V.; Gonzalez-Nilo, F. D. Block Copolymers in the Synthesis of Gold Nanoparticles. Two New Approaches: Copolymer Aggregates as Reductants and Stabilizers and Simultaneous Formation of Copolymer Aggregates and Gold Nanoparticles. *J. Polym. Sci., Part A: Polym. Chem.* **2014**, *52*, 3069−3079.
(39) Klauda, J. B.; Venable, R. M.; Freites, J. A.; O'Connor, J. W.; Tobias, D. J.; Mondragon-Ramirez, C.; Vorobyov, I.; MacKerell, A. D., Jr.; Pastor, R. W. Update of the CHARMM all-atom additive force field for lipids: validation on six lipid types. *J. Phys. Chem. B* **2010**, *114*, 7830−7843.
(40) Vorobyov, I.; Anisimov, V. M.; Greene, S.; Venable, R. M.; Moser, A.; Pastor, R. W.; MacKerell, A. D. Additive and Classical Drude Polarizable Force Fields for Linear and Cyclic Ethers. *J. Chem. Theory Comput.* **2007**, *3*, 1120−1133.
(41) Jorgensen, W. L.; Chandrasekhar, J.; Madura, J. D.; Impey, R. W.; Klein, M. L. Comparison of Simple Potential Functions for Simulating Liquid Water. *J. Chem. Phys.* **1983**, *79*, 926−935.
(42) Phillips, J. C.; Braun, R.; Wang, W.; Gumbart, J.; Tajkhorshid, E.; Villa, E.; Chipot, C.; Skeel, R. D.; Kale, L.; Schulten, K. Scalable molecular dynamics with NAMD. *J. Comput. Chem.* **2005**, *26*, 1781−1802.
(43) Humphrey, W.; Dalke, A.; Schulten, K. VMD: visual molecular dynamics. *J. Mol. Graphics* **1996**, *14*, 33−38.
(44) Martyna, G. J.; Tobias, D. J.; Klein, M. L. Constant-Pressure Molecular-Dynamics Algorithms. *J. Chem. Phys.* **1994**, *101*, 4177−4189.
(45) Andersen, H. C. Rattle - a Velocity Version of the Shake Algorithm for Molecular- Dynamics Calculations. *J. Comput. Phys.* **1983**, *52*, 24−34.
(46) Essmann, U.; Perera, L.; Berkowitz, M. L.; Darden, T.; Lee, H.; Pedersen, L. G. A Smooth Particle Mesh Ewald Method. *J. Chem. Phys.* **1995**, *103*, 8577−8593.
(47) Marrink, S. J.; Risselada, H. J.; Yefimov, S.; Tieleman, D. P.; de Vries, A. H. The MARTINI force field: coarse grained model for biomolecular simulations. *J. Phys. Chem. B* **2007**, *111*, 7812−7824.
(48) Lee, H.; De Vries, A. H.; Marrink, S. J.; Pastor, R. W. A coarse-grained model for polyethylene oxide and polyethylene glycol: conformation and hydrodynamics. *J. Phys. Chem. B* **2009**, *113*, 13186−13194.
(49) Lee, H.; Pastor, R. W. Coarse-grained model for PEGylated lipids: effect of PEGylation on the size and shape of self-assembled structures. *J. Phys. Chem. B* **2011**, *115*, 7830−7837.
(50) Zhu, A.; Weng, J.; Liu, Q. Mechanism analysis of poly(lactic acid) particles formation by mesoscale simulation. *J. Appl. Polym. Sci.* **2011**, *119*, 3273−3281.
(51) Sadowski, G., Richtering, W., Eds. *Intelligent Hydrogels*; Springer: Cham, Switzerland, 2013.
(52) Periole, X.; Marrink, S. J. The Martini coarse-grained force field. *Methods Mol. Biol.* **2013**, *924*, 533−565.
(53) Hess, B.; Kutzner, C.; van der Spoel, D.; Lindahl, E. GROMACS 4: Algorithms for Highly Efficient, Load-Balanced, and Scalable Molecular Simulation. *J. Chem. Theory Comput.* **2008**, *4*, 435−447.
(54) Berendsen, H. J. C.; Postma, J. P. M.; Vangunsteren, W. F.; Dinola, A.; Haak, J. R. Molecular-Dynamics with Coupling to an External Bath. *J. Chem. Phys.* **1984**, *81*, 3684−3690.
(55) Thota, N.; Jiang, J. Self-assembly of amphiphilic peptide (AF) 6H5K15 derivatives: roles of hydrophilic and hydrophobic residues. *J. Phys. Chem. B* **2014**, *118*, 2683−2692.

DOI: 10.1021/acs.langmuir.6b02177
Langmuir 2016, 32, 7929−7942